Volume 3
Number 10
October 2024
Pages 1581–1760

Sensors & Diagnostics

rsc.li/sensors

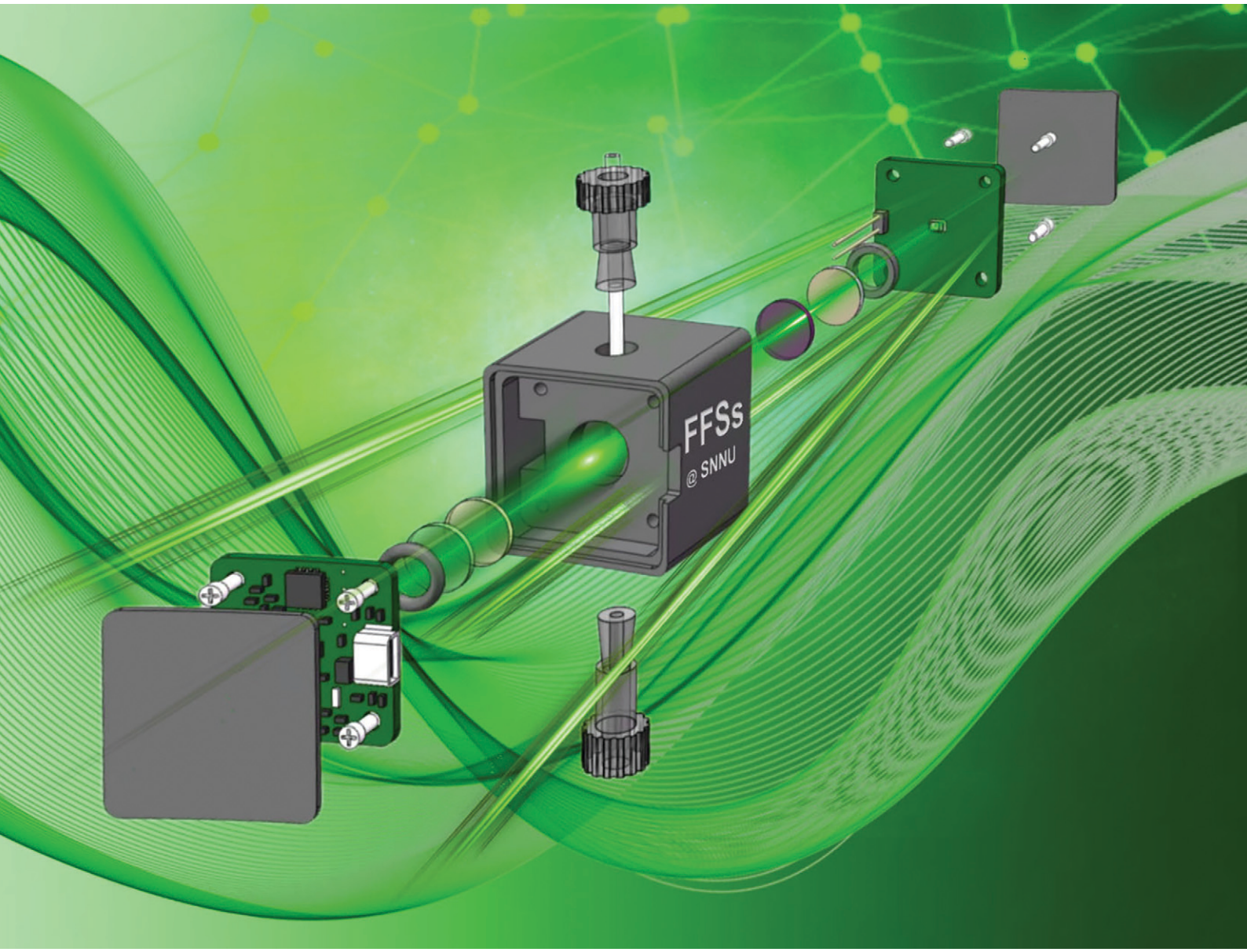

ISSN 2635-0998

ROYAL SOCIETY OF CHEMISTRY

PAPER
Taihong Liu, Molin Qin, Zhiyan Huang *et al.*
Compact device prototype for turn-on fluorescence detection of sarin based on reactive 4,4-diaryloxy-BODIPY derivatives

Sensors & Diagnostics

PAPER

View Article Online
View Journal | View Issue

Cite this: *Sens. Diagn.*, 2024, **3**, 1651

Compact device prototype for turn-on fluorescence detection of sarin based on reactive 4,4-diaryloxy-BODIPY derivatives†

Lu Liu,‡[a] Sheng Li,‡[a] Wendan Luo,[a] Jiashuang Yao,[a] Taihong Liu, *[a] Molin Qin,*[b] Zhiyan Huang,*[a] Liping Ding [a] and Yu Fang [a]

Received 27th June 2024,
Accepted 5th September 2024

DOI: 10.1039/d4sd00228h

rsc.li/sensors

Development of fluorescence indicators for efficient and accurate detection of lethal nerve agents has evoked extensive interest recently. Herein, we presented two spiranic 4,4-diaryloxy-BODIPY derivatives for efficient and fluorescence turn-on detection of sarin in solution media. A colorimetric mode featured the merits of obvious color changes from dark to greenish fluorescence under UV light. The generated new fluorescence emissions reached their maxima within several minutes and the peaks were assigned to the generated by-product oxo-BDP with a fluorescence quantum yield (Φ_F) ~ 20% in acetonitrile. The detection limits of two 4,4-diaryloxy-BODIPYs for a simulant diethylchlorophosphate (DCP) were determined to be 13.2 nM and 8.2 nM, respectively. The underlying sensing mechanism was clarified as the synergistic effect of 4,4-bond cleaving and fluorescence turn-on related to the photoinduced electron transfer process. Furthermore, a compact tubular sensor and a sensing platform prototype were fabricated properly. Superior detection results and further evaluation for real samples and simulants could be conducted at the sub-mM level on-site. Successful trials aid in understanding the structure–function relationship of 4,4-disubstituted BODIPY chromophores as well as the future development of a miniaturized device prototype for on-site detection of chemical warfare agents.

Nerve agents as dangerous and lethal chemical warfare agents (CWAs) have been banned by the Organization for the Prohibition of Chemical Weapons (OPCW).[1,2] Their electrophilic phosphate group irreversibly binds with the hydroxyl group of the serine residue of acetylcholinesterase (AChE), resulting in central nervous system paralysis, organ failure, and rapid fatality.[3–6] Among the classified G- and V-type nerve agents and the most recent Novichok agents, the severe sarin (GB), which has been employed in various terrorist incidents, gains special attention.[7] Therefore, extensive efforts have been made in developing facile, selective, and reliable methods for detecting nerve agents to ensure public and national safety in recent years. The field of rapid screening and *in situ* detection of CWAs has experienced noticeable growth but is still challenging. Conventional methods such as ion mobility spectrometry, gas chromatography, chemiresistors, and electrochemical techniques may suffer from inherent limitations including limited selectivity, high cost, labor-intensive protocols, and sophisticated instrumentation.[8–13] Nowadays, optical techniques offer distinct advantages for their operational simplicity, inherent high sensitivity, low-cost implications, facile real-time analysis capabilities, ease of manipulation, and suitability for field detection applications.[14–21] Among various methods, colorimetric and fluorogenic chemosensors have attracted great attention due to the advantages of exceptional sensitivity, rapid response, and user-friendly operation (Table S1†).[22–25] The recent advances of fluorescence and colorimetric chemosensors for detecting CWAs has been reviewed by Churchill,[1] Kumar, James, Yoon, Anslyn, *et al.*[2,23,26] However, high selectivity towards the specific targeting CWA analyte is often difficult to achieve. On the other hand, the turn-off detection mechanism for the majority of chemosensors could bring about unsatisfactory disruptions caused by photobleaching or conventional aggregation-caused quenching.[27] Therefore, innovative sensing indicators not only endow output signals but also determine the sensing

[a] *Key Laboratory of Applied Surface and Colloid Chemistry of Ministry of Education, School of Chemistry and Chemical Engineering, Shaanxi Normal University, Xi'an 710119, P. R. China. E-mail: liuth121@snnu.edu.cn, zyhuang@snnu.edu.cn*
[b] *State Key Laboratory of NBC Protection for Civilian, Beijing 102205, P. R. China. E-mail: qinmolin@139.com*

† Electronic supplementary information (ESI) available: General synthesis procedures, single crystal analysis, structural characterization, optical spectra, additional NMR and HRMS spectra, *etc.* CCDC 2367202. For ESI and crystallographic data in CIF or other electronic format see DOI: **https://doi.org/10.1039/d4sd00228h**

‡ L. L. and S. L. contributed equally to this work.

effectiveness, and the development of novel chromo-fluorogenic indicators is still highly desired.

Boron dipyrromethenes (BODIPYs) with high photochemical stability and fluorescence efficiency form one of the most important families of organic chromophores. Their strong absorption and high fluorescence up to the near-infrared spectral region make them desirable for various applications, particularly as fluorescence labels and sensors.[28–31] Similarly, general functional strategies of BODIPYs focused on introducing an oximido-group,[32] amine,[33,34] hydroxy,[16,35,36] or pyridyl segment due to their effective nucleophilicity towards the electrophilic phosphate group, resulting in the colorimetric and/or fluorescence signal changes.[7,26,37] Relevant reaction of BODIPYs with nerve agents resulted in the phosphorylation of the hydroxy unit and subsequent intramolecular *N*-alkylation to form the corresponding morpholino cations or five-membered-ring quaternary ammonium salts.[2] As a unique example, Martínez-Máñez *et al.* prepared a BODIPY dye containing three reactive sites; (i) a nucleophilic phenol group able to undergo phosphorylation with nerve agents, (ii) a carbonyl group as a reactive site for cyanide, and (iii) a triisopropylsilyl protecting group that was known to react with fluoride. This first enabled colorimetrically differentiating between DCNP (a tabun simulant) and DFP (a sarin and soman simulant).[38] On the other hand, their photophysical properties can be easily modulated *via* straightforward functionalization of the rich BODIPY chemistry. Mostly, the introduction of certain groups and functionalities at the 2-/6-, 3-/5-, or 8-positions of the dipyrromethene core allows for extended π-conjugation systems.[39] Kim *et al.* reported a turn-on fluorogenic probe *o*-OH to detect and quantify organophosphorus nerve agent mimics by suppressing the internal rotation upon phosphorylation of a reactive phenolate in BODIPY.[16] Versatile functionalization at the boron center (4,4-position) normally has little effect on the spectroscopic properties, but can be used to enlarge the Stokes shifts and finely tune the fluorescence quantum yield of the resultant BODIPYs.[29,39,40] Martínez-Martínez *et al.* demonstrated the manipulative push–pull character of a family of BINOL-based *O*-BODIPYs comprehensively, explaining the abnormally dramatic loss of the fluorescence in some chromophores.[28] Moreover, the 4,4-dialkoxy positions could be further employed as reactive sites for some hazardous analytes. Inspired by the restoration of BODIPY's intrinsic fluorescence following the 4,4-bond cleavage under mildly harsh conditions, we have ingeniously devised a turn-on fluorescence sensing approach (Fig. 1a).

Herein, two innovative 4,4-diaryloxy-BODIPY derivatives denoted as OBP1 and OBP2 were obtained following a one-step strategy (Fig. 1b; Scheme S1†).[27,29,30] The single crystal of the compound OBP1 cultivated in CH_2Cl_2/*n*-hexane was examined properly (Table S2†) and it belonged to a triclinic $P\bar{1}$ space group (Fig. S1†). Both indicators underwent a substitution reaction upon interacting with the simulant diethylchlorophosphate (DCP) in solution media, generating a greenish fluorescence under UV light.[28,41,42] Inspired by the interesting findings and the research background in our group, a tubular, laminated, and low-power sensor was integrated properly. Then a sensing platform prototype was further fabricated and applied for on-site detection of sarin and its simulants at the sub-mM level. The underlying sensing mechanism was clarified as the synergistic effect of

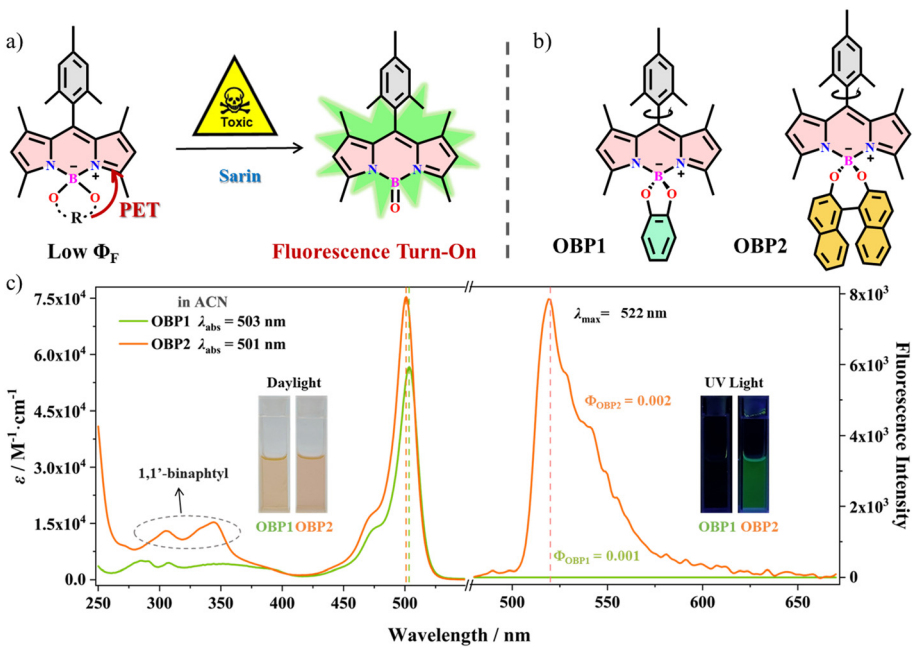

Fig. 1 (a) Proposed strategy based on the reactive 4,4-diaryloxy-BODIPY derivatives for detecting sarin. (b) Chemical structures of the spiranic 4,4-diaryloxy-BODIPY derivatives OBP1 and OBP2. (c) UV-vis absorption and fluorescence emission spectra of OBP1 and OBP2 in ACN ($c \sim 8.0 \times 10^{-6}$ M); inset shows the colors of their solutions under daylight and UV light (365 nm).

the bond cleaving at the 4,4-position and the fluorescence recovery related to the photoinduced electron transfer (PET) in the resultant by-product.

Optical properties of the spiranic 4,4-diaryloxy-BODIPY derivatives

The basic photophysical properties of OBP1 and OBP2 in ACN were first investigated (Fig. S2 and S3;† Table S3†). Typical UV-vis absorption maxima (λ_{max}) of the spiranic 4,4-diaryloxy-BODIPYs around 500 nm corresponded to the π–π* transition along the BODIPY axis with significant molar extinction coefficients (Fig. 1c). The key parameters agreed with previous reports regarding that substitution of fluorides in BODIPY dyes with alkoxy groups, illustrating the minor effect of the spiranic 4,4-diaryloxyl units to the electronic energy of the target derivatives.[27,43] Additional weak and broad absorption bands at 275–375 nm should be ascribed to the electron-donating groups of the 1,2-benzenediol or 1,1′-binaphthyl unit.[44] In detail, OBP2 exhibited an absorption maximum at 501 nm and an emission maximum at 522 nm in ACN ($\Delta\lambda$ = 21 nm). The molecular coefficient (ε) and optical energy gap (E_g) values were found to be 6.53 × 10^4 M^{-1} cm^{-1} and 2.39 eV, respectively. The additional characteristic bands at 275–375 nm were typically for the 1,1′-binaphthyl unit.[45] We speculated that its low fluorescence quantum yield (Φ_F) value ~0.01 in ACN should be attributed to PET and its efficient interactions with the surrounding solvent, resulting in non-radiative decay processes.[46,47] Both spiranic 4,4-diaryloxy-BODIPY derivatives in kinds of organic solvents exhibited similar absorption maxima ranging from 501 to 510 nm, and OBP2 emitted fluorescence emission around 525 nm with slight solvent effects (Fig. S3;† Table S3†).

Sensing characteristics of both 4,4-dialkoxy-BODIPY derivatives to the simulant DCP

Upon adding DCP to the desired OBP1 in ACN, its absorption maximum at 503 nm decreased immediately (Fig. S4a†), and the linear relationship of the absorbance ($A_{503\ nm}$) and the concentration of DCP was found to be $y = -0.05 \times c_{DCP} + 0.46$

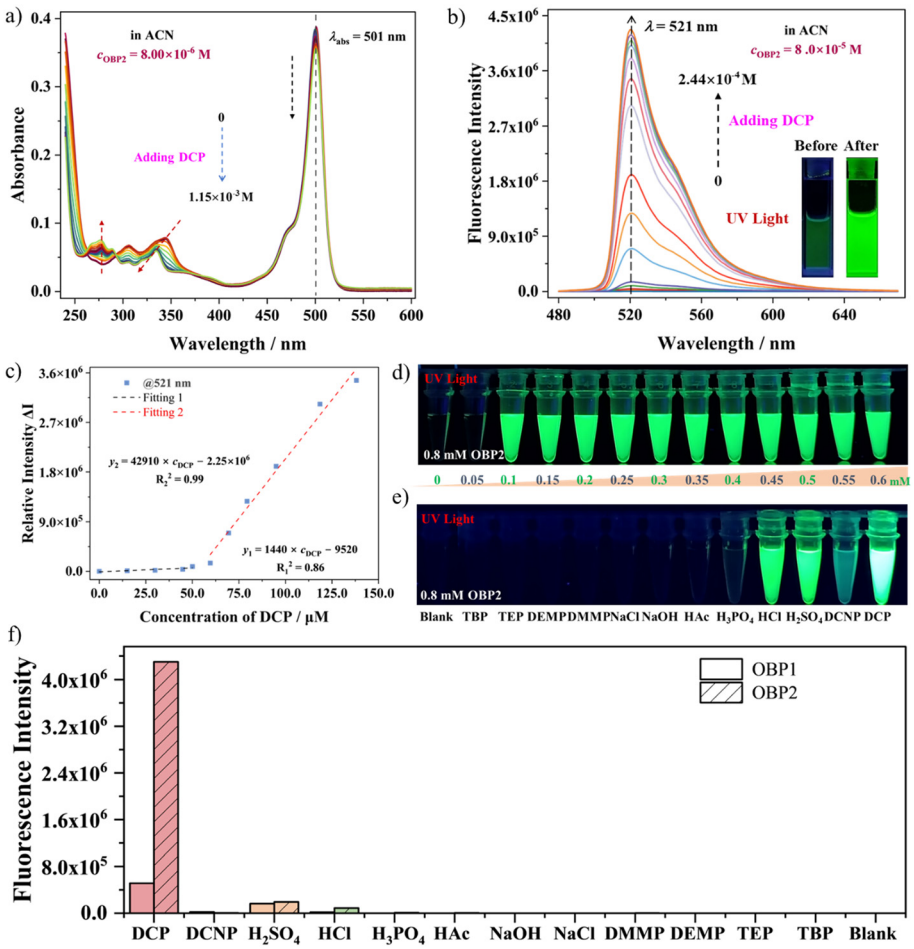

Fig. 2 (a) Concentration-dependent UV-vis absorption spectra of OBP2 (c ~ 8.0 ×10^{-6} mol L^{-1}) with increasing DCP in ACN. (b) Fluorescence emission spectra of OBP2 (c ~ 8.0 ×10^{-5} mol L^{-1}) in ACN upon adding DCP. Inset shows the fluorescence color changes. (c) Fluorescence intensity plot of OBP2 (c ~ 8.0 ×10^{-5} mol L^{-1}) at 521 nm with increasing concentrations of DCP. (d) Obvious fluorescence color changes of OBP2 (c ~ 0.8 mM) toward different concentrations of DCP. (e) Obvious fluorescence color changes of OBP2 (c ~ 0.8 mM) toward different analytes. (f) Selectivity performance of the two indicators to DCP (c ~ 0.08 mM) and other interferences (c ~ 0.32 mM).

(coefficient R^2 = 0.998, Fig. S4b†). The solution color changed from pink to yellowish gradually under daylight. While under UV light, OBP1 showed a turn-on fluorescence emission at 521 nm, ascribed to a newly generated by-product oxo-BDP (4-(oxo) borane-1,3,5,7-tetramethyl-8-(2′,4′,6′-trimethylbenzene)), which was confirmed below (Fig. S4c†). A satisfactory linear relationship of fluorescence emission intensity changes ($\Delta I = I - I_0$) at 521 nm with the concentration of DCP was also found (Fig. S4d†). And the detection limit (DL) value of OBP1 to DCP was calculated to be 13.2 nM in terms of the $3\sigma/k$ equation.

Differently, the absorption maximum of OBP2 around 501 nm changed negligibly upon adding DCP, accompanied only by the slight increase of the band around 275 nm (Fig. 2a). Interestingly, OBP2 exhibited a fast and turn-on fluorescence response at 521 nm maximum to DCP. Related greenish fluorescence under UV light could be easily observed by the naked eye (Fig. 2b and d). The Φ_F value of the generated intermediate oxo-BDP was determined to be 0.197. Upon increasing the DCP concentrations up to 130.0 μM, a total of two linear stages of the fluorescence intensity at 521 nm were found (Fig. 2c). The first-stage relationship slope was fitted within the concentration ranging from 0 to 50.0 μM (coefficient R^2 = 0.86), and that of the second-stage was fitted satisfactorily within the concentration range of 50.0–130.0 μM (R^2 = 0.99). The low DL value of OBP2 to DCP was determined to be 8.2 nM in terms of the typical $3\sigma/k$ equation (Fig. 2c). In our opinion, the two stages might be ascribed to the two phosphorylation steps at the oxygen atoms of the spiranic 4,4-diaryloxy-BODIPYs. The first binding of an electrophilic phosphate group formed an intermediate with the partially blocked PET process and thus recovered a portion of fluorescence emission.[48] The second phosphorylation accelerated the cleaving reaction to lose the diethyl phosphate group and generated the intermediate oxo-BDP, thereby exhibiting a better fluorescence enhancement for a higher DCP concentration.

We know that response time and detection selectivity are vital parameters to evaluate the capability of active indicators. Adding different folds of DCP to OBP2 in ACN, the fluorescence intensity increased rapidly in a couple of minutes and remained stable in a longer stand-by time. Based on the time-dependent measurement analysis, the reaction time was optimized to be 5.0 min (Fig. S5†). To further inspect their selectivity, organophosphorus interferents like diethyl cyanophosphonate (DCNP), triethyl phosphate (TEP), tributyl phosphonate (TBP), diethyl methylphosphonate (DEMP), and dimethyl methylphosphonate (DMMP) were of analytical grade and used as received. As shown in Fig. 2f, the interferents DCNP, TBP, TEP, DEMP, and DMMP showed little effect on the fluorescence detection. Other interferents like NaCl, NaOH, HAc, and H_3PO_4 ($c \sim 0.32$ mM) supported the good selectivity of both indicators for DCP detection. Meanwhile, dramatic greenish fluorescence changes with DCNP, H_2SO_4 and HCl under UV light were an imperfect illustration for DCP sensing (Fig. 2e). If compared with the reported results, the present strategy with good sensing parameters possessed great application potential in detecting sarin (Table S1†).

Underlying sensing mechanism investigations

The quick and obvious observation of registered fluorescence emission indicated the reaction between DCP and the 4,4-dialkoxy-BODIPYs (Fig. 3a). In our opinion, the 4,4-dialkoxy-BODIPYs were fluorescence silent through the PET mechanism. In the presence of DCP, the 4,4-dialkoxy-BODIPYs reacted with DCP through a nucleophilic substitution reaction firstly to form a phosphorylated intermediate. Then a cleaving reaction to lose the diethyl phosphate group followed to generate the by-product oxo-BDP that exhibited an obvious turn-on fluorescence response.[49,50] In this way, both OBP1 and OBP2 generated the same oxo-BDP with a similar fluorescence emission maxima at 521 nm (Fig. 2c and S4†). To confirm the detection mechanism, we obtained the mass spectra of the mixture of indicators with DCP. In contrast to the MALDI-TOF mass peak of OBP2 at 612.2 MW (Fig. 3b), a newly generated peak at 344.9 MW should be assigned to a new by-product oxo-BDP after the removal of the spiranic diaryloxy unit (Fig. 3c). We also isolated the generated intermediate 1,1′-binaphthalene-2,2′-diyltetraethyl bis(phosphate) unit and characterized it by NMR (Fig. S6†). The phosphorylation process to the 1,1′-binaphthyl-2,2′-diol unit laterally evidenced the plausible sensing mechanism. It is well supported that the present detection was achieved by the generation of a new intermediate oxo-BDP without the PET effect, resulting in a "turn-on" fluorescence response.[46] Similar MALDI-TOF mass results achieved from OBP1 also supported the conversion of 4,4-dialkoxy-BODIPY derivatives to the by-product oxo-BDP (Fig. S7†).

Construction of the compact device

Inspired by the findings and the research foundation in our group, a tubular, laminated, and low-power sensor was integrated first (Fig. 4a).[51–54] The unique laminated structure endows the sensory unit with enhanced sensing performance and kinetics discriminability to discriminate analytes. In detail, the small-sized sensor (3 × 3 × 2 cm^3, weight ~ 34.0 g) was assembled with a photodiode light with ~460 nm excitation illumination (FWHM ~ 30 nm), a tubular sample pool, narrowband optical filters, and solid-state photomultiplier (SSPM, ~520 nm/FWHM 40 nm) readout unit (Fig. 4b). The optical densities of the filters #1 and #2 were OD4 and OD6, respectively. Furthermore, a compact prototype composed of a sensory unit, a double-throw switch control module, mini pumps, a digital display system, pulse sampling inlets and waste collecting systems (Fig. 4c and d) was fabricated properly. Flowing samples was managed by the mini pump and the double-throw switch control module. The atmospheric pressure, environment temperature and humidity were recorded properly using the environmental monitoring system. Superior to professional laboratory instruments, *in situ* and continuous evaluation could be conducted efficiently. Moreover, valuable response kinetics could also be recorded, which favors analyzing the interactions between the analytes and the sensing indicators.[55,56]

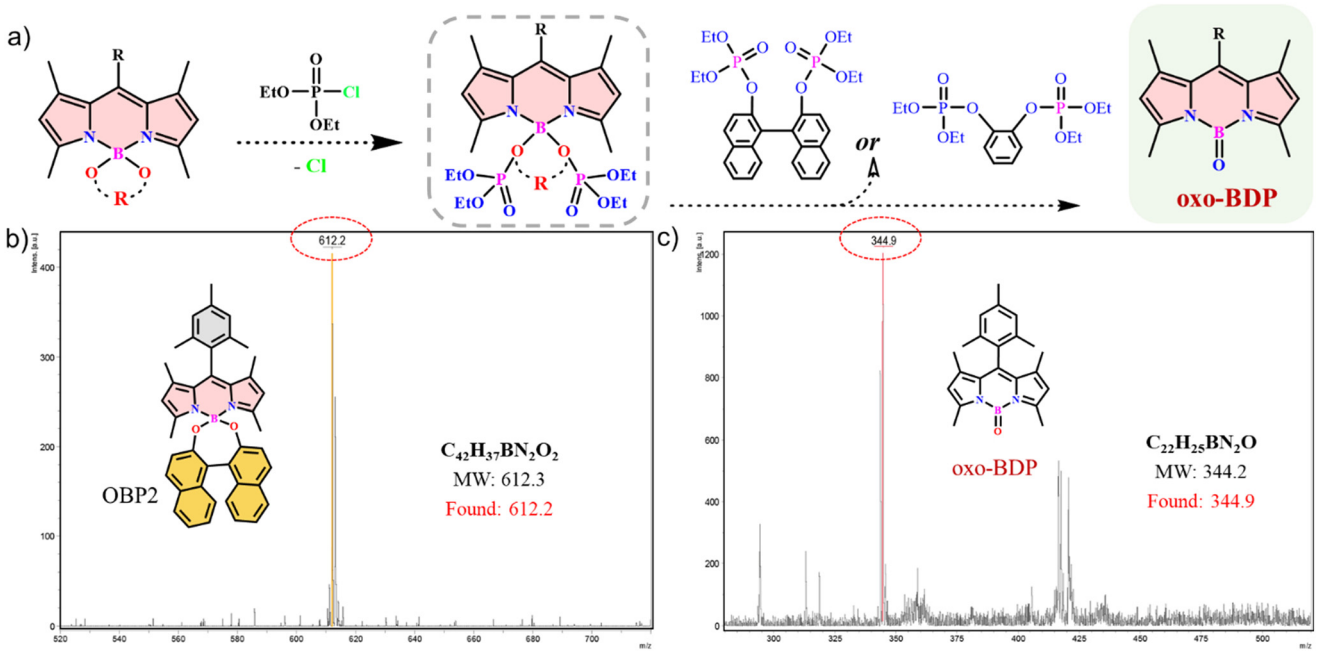

Fig. 3 (a) Plausible sensing mechanism for the reactive 4,4-dialkoxy-BODIPY derivatives to detect DCP. (b) MALDI-TOF spectrum of OBP2 (theoretical M_W = 612.3). (c) MALDI-TOF spectrum of the plausible generated oxo-BDP, 4-(oxo)borane-1,3,5,7-tetramethyl-8-(2′,4′,6′-trimethylbenzene) (theoretical M_W = 344.2).

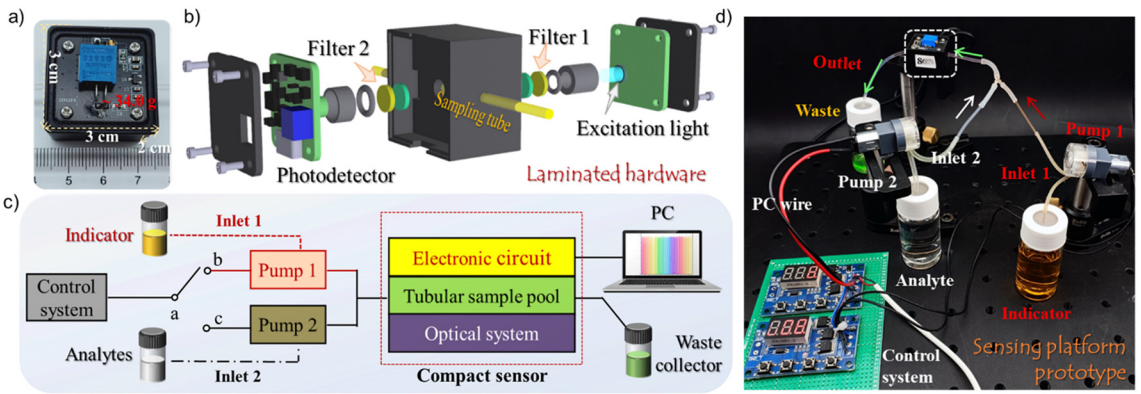

Fig. 4 Photograph (a) and exploded view (b) of the laminated tubular sensor. Schematic representation (c) and picture (d) of the home-made sensing platform.

Before the testing, wavelet denoising and baseline correction were conducted and a blank signal I_0 was obtained using a control solution. Then, the analyte was pumped into the sampling system and detectable signal changes at 521 nm as I were monitored. Therefore, the difference value between I_0 and I (ΔI_{521}) represented the sensing signal or the response intensity of one analyte. A linear relationship of ΔI_{521} values was found with changing the analyte concentrations. The response traces of OBP2 to DCP (0–30.0 μM) are illustrated in Fig. 5a with a good linear relationship of $y = 5571.8 \times c_{DCP} - 4192.1$ (R^2 = 0.996, Fig. 5b). The sensing performance of OBP1 to DCP (0–150.0 μM) was observed in Fig. S8† (R^2 = 0.994). The relative standard deviation (RSD) was as low as 3.04% for 55 batch-to-batch detection cycles, proving the outstanding stability and favorable reproducibility of the present sensing platform (Fig. 5c). Distinguishability is a crucial factor for determining the real-life applicability of a device prototype. In contrast to the remarkable response of DCP, other potential interferents like TBP, TEP, DEMP, DMMP, *etc.* displayed negligible effect on the sensing performance (Fig. 5d).

Detection and identification of the nerve agent sarin

We also evaluated the potential *in situ* applicability of the sensing platform prototype to further field applications. Sensing results of the nerve agent sarin (GB) were carried out properly (Fig. 6 and S9†). Excellent response intensity plots of OBP2 ($c = 8.0 \times 10^{-5}$ M) against sarin well fitted with a

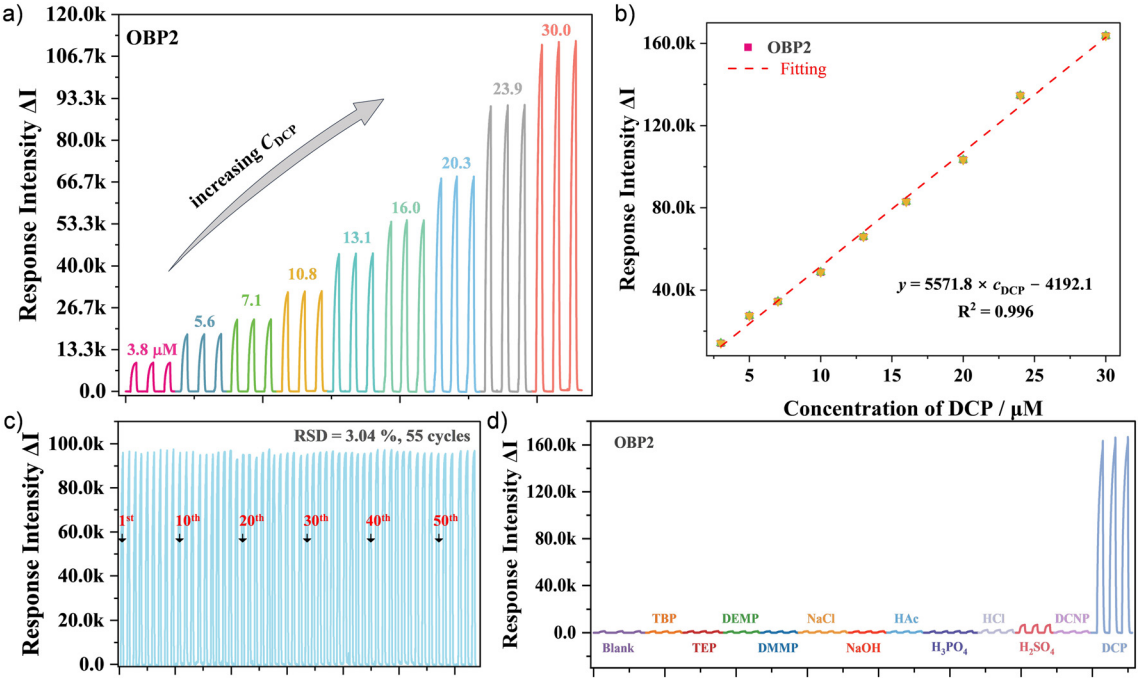

Fig. 5 (a) Response traces of OBP2 in ACN to different concentrations of DCP conducted by the compact device (note: each test was repeated at least three times). (b) Response plot and linear fitting of OBP2 to different concentrations of DCP. (c) Sensing reversibility and stability tests of the sensing platform toward DCP with 55 cycles. (d) Response selectivity of OBP2 to the presence of different potential interferents ($c \sim 30.0$ μM).

correlation coefficient of 0.992 (Fig. 6a and b). And the DL value for sarin was determined to be 2.04×10^{-5} mol L^{-1}, which was well below the hazardous concentration. Dramatic greenish fluorescence illustrations of both spiranic 4,4-diaryloxy-BODIPYs under UV light were obtained with gradually increasing the concentration of sarin (Fig. 6c and d), supporting the possible dual-mode visualized detection.[57] The fast response and direct measurements satisfied the field requirements without additional processing or complicated sample enrichment. It is believed that the as-prepared fluorescence indicator as well as the device platform will greatly contribute to development in the related fields.

Conclusions

Two spiranic 4,4-diaryloxy-BODIPYs (OBP1 and OBP2) were proven to be high-performance fluorescent materials. Their emission responses were highly sensitive to the presence of

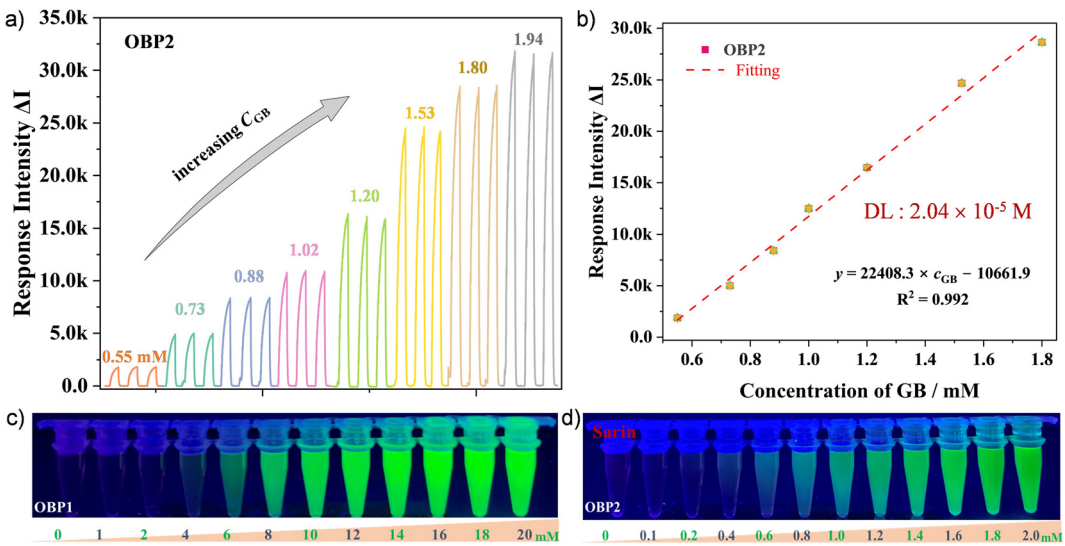

Fig. 6 (a) Response traces of OBP2 in ACN to different concentrations of GB conducted by the home-made compact device prototype. (b) Response plot and linear fitting of OBP2 to different concentrations of GB. Fluorescence color changes of compound OBP1 (c) and OBP2 (d) to sarin (GB).

DCP, showing a remarkable fluorescence color change to bright green within 5 minutes. Generated new fluorescence emission peaks were assigned for the generated by-product oxo-BDP with a moderate fluorescence quantum yield. The plausible sensing mechanism was clarified as the synergistic effect of 4,4-bond cleaving and fluorescence recovery of BODIPYs related to the absence of PET. Furthermore, a laminated tubular sensor and a compact device prototype were fabricated properly. The unique laminated structure endowed the sensory unit with good efficiency, high sensitivity, and device robustness to discriminate analytes. Superior detection parameters and continuous on-site evaluation for sarin were conducted at the sub-mM level in solution media. This study presents a new and efficient fluorescence method for sensing sarin and simulants. Furthermore, the presented strategy as a conceptual proof-of-principle research will inspire the exploration of novel portable systems for the online and *in situ* detection of CWAs.

Data availability

The details on general synthesis procedures, single crystal analysis, structural characterization, optical spectra, additional NMR and HRMS spectra, *etc.* are available in the ESI† as provided.

Author contributions

L. L. and S. L. contributed equally to this work. The manuscript was written through contributions of all authors. L. L. and S. L. performed all experimental work and data analysis and wrote the original draft. W. L. and J. Y. analyzed the data. M. Q. and Z. H. analyzed the data and corrected the manuscript. T. L. supervised the project, analyzed the data, and wrote the manuscript. L. D. and Y. F. analyzed the data and corrected the manuscript.

Conflicts of interest

There are no conflicts of interest to declare.

Acknowledgements

The authors acknowledge the financial funding from the National Key Research and Development Program of China (2022YFA1205502), the National Natural Science Foundation of China (22172097 and 21820102005), the 111 Project (B14041), and the China Agriculture Research System (CARS-27).

Notes and references

1 Y. J. Jang, K. Kim, O. G. Tsay, D. A. Atwood and D. G. Churchill, *Chem. Rev.*, 2015, **115**, PR1-PR76.
2 W.-Q. Meng, A. C. Sedgwick, N. Kwon, M. Sun, K. Xiao, X.-P. He, E. V. Anslyn, T. D. James and J. Yoon, *Chem. Soc. Rev.*, 2023, **52**, 601–662.
3 M. Lafuente, D. Sanz, M. Urbiztondo, J. Santamaría, M. P. Pina and R. Mallada, *J. Hazard. Mater.*, 2020, **384**, 121279.
4 W. Meng, Z. Pei, Y. Wang, M. Sun, Q. Xu, J. Cen, K. Guo, K. Xiao and Z. Li, *J. Hazard. Mater.*, 2021, **410**, 124811.
5 M.-J. Xue, X.-Z. Wei, W. Feng, Z.-F. Xing, S.-L. Liu and Q.-H. Song, *J. Hazard. Mater.*, 2021, **416**, 125789.
6 V. Kumar, *Chem. Commun.*, 2021, **57**, 3430–3444.
7 T. Sultana, M. Mahato, S. Ahamed, N. Tohora, J. Chourasia, S. Ali and S. K. Das, *Sens. Diagn.*, 2024, **3**, 1285–1297.
8 I. Bhowmick and Neelam, *Analyst*, 2014, **139**, 4154–4168.
9 B. Díaz de Greñu, D. Moreno, T. Torroba, A. Berg, J. Gunnars, T. Nilsson, R. Nyman, M. Persson, J. Pettersson, I. Eklind and P. Wästerby, *J. Am. Chem. Soc.*, 2014, **136**, 4125–4128.
10 A. M. Costero, S. Gil, M. Parra, P. M. E. Mancini, R. Martínez-Máñez, F. Sancenón and S. Royo, *Chem. Commun.*, 2008, 6002–6004.
11 A. Wild, A. Winter, M. D. Hager and U. S. Schubert, *Chem. Commun.*, 2012, **48**, 964–966.
12 V. Schroeder, S. Savagatrup, M. He, S. Lin and T. M. Swager, *Chem. Rev.*, 2019, **119**, 599–663.
13 S.-O. Kim, S. G. Kim, H. Ahn, J. Yoo, J. Jang and T. H. Park, *ACS Sens.*, 2023, **8**, 3095–3103.
14 Q. Liu, T. Liu and Y. Fang, *Langmuir*, 2020, **36**, 2155–2169.
15 K. Liu, J. Zhang, L. Xu, J. Liu, L. Ding, T. Liu and Y. Fang, *Chem. Commun.*, 2019, **55**, 12679–12682.
16 T.-I. Kim, S. B. Maity, J. Bouffard and Y. Kim, *Anal. Chem.*, 2016, **88**, 9259–9263.
17 J. Zhang, K. Liu, Z. Liu, Z. Wang, C. Hua, T. Liu and Y. Fang, *ACS Appl. Mater. Interfaces*, 2021, **13**, 5625–5633.
18 Z. Wang, G. Wang, X. Chang, K. Liu, Y. Qi, C. Shang, R. Huang, T. Liu and Y. Fang, *Adv. Funct. Mater.*, 2019, **29**, 1905295.
19 J. Yao, Y. Fu, W. Xu, T. Fan, Y. Gao, Q. He, D. Zhu, H. Cao and J. Cheng, *Anal. Chem.*, 2016, **88**, 2497–2501.
20 E. Singh, M. Meyyappan and H. S. Nalwa, *ACS Appl. Mater. Interfaces*, 2017, **9**, 34544–34586.
21 M. S. J. Khan, Y.-W. Wang, M. O. Senge and Y. Peng, *J. Hazard. Mater.*, 2018, **342**, 10–19.
22 T. Liu, L. Yang, W. Feng, K. Liu, Q. Ran, W. Wang, Q. Liu, H. Peng, L. Ding and Y. Fang, *ACS Appl. Mater. Interfaces*, 2020, **12**, 11084–11093.
23 L. Chen, D. Wu and J. Yoon, *ACS Sens.*, 2018, **3**, 27–43.
24 L. Zeng, H. Zeng, L. Jiang, S. Wang, J.-T. Hou and J. Yoon, *Anal. Chem.*, 2019, **91**, 12070–12076.
25 X. Zhou, Y. Zeng, C. Liyan, X. Wu and J. Yoon, *Angew. Chem., Int. Ed.*, 2016, **55**, 4729–4733.
26 V. Kumar, H. Kim, B. Pandey, T. D. James, J. Yoon and E. V. Anslyn, *Chem. Soc. Rev.*, 2023, **52**, 663–704.
27 L. Gartzia-Rivero, E. M. Sánchez-Carnerero, J. Jiménez, J. Bañuelos, F. Moreno, B. L. Maroto, I. López-Arbeloa and S. de la Moya, *Dalton Trans.*, 2017, **46**, 11830–11839.
28 J. Jiménez, R. Prieto-Montero, B. L. Maroto, F. Moreno, M. J. Ortiz, A. Oliden-Sánchez, I. López-Arbeloa, V. Martínez-Martínez and S. de la Moya, *Chem. – Eur. J.*, 2020, **26**, 601–605.

29 A. Blázquez-Moraleja, D. Álvarez-Fernández, R. Prieto Montero, I. García-Moreno, V. Martínez-Martínez, J. Bañuelos, I. Sáenz-de-Santa-María, M. D. Chiara and J. L. Chiara, *Dyes Pigm.*, 2019, **170**, 107545.
30 K. Kim, O. G. Tsay, D. A. Atwood and D. G. Churchill, *Chem. Rev.*, 2011, **111**, 5345–5403.
31 L. Liu, S. Li, N. Zhang, Q. Shi, K. Liu, T. Liu, Z. Huang, L. Ding and Y. Fang, *J. Phys. Chem. B*, 2023, **127**, 10171–10178.
32 Y. J. Jang, O. G. Tsay, D. P. Murale, J. A. Jeong, A. Segev and D. G. Churchill, *Chem. Commun.*, 2014, **50**, 7531–7534.
33 L. Zeng, T. Chen, B. Zhu, S. Koo, Y. Tang, W. Lin, T. D. James and J. S. Kim, *Chem. Sci.*, 2022, **13**, 4523–4532.
34 F. W. Dagnaw, Y.-P. Cai and Q.-H. Song, *Dyes Pigm.*, 2021, **189**, 109257.
35 T. Chen, L. Jiang, J.-T. Hou, W. Wang, L. Zeng and G.-M. Bao, *J. Mater. Chem. A*, 2020, **8**, 24695–24702.
36 Z.-N. Sun, F.-Q. Liu, Y. Chen, P. K. H. Tam and D. Yang, *Org. Lett.*, 2008, **10**, 2171–2174.
37 Q. Chen, J. Liu, S. Liu, J. Zhang, L. He, R. Liu, H. Jiang, X. Han and K. Zhang, *Anal. Chem.*, 2023, **95**, 4390–4394.
38 A. Barba-Bon, A. M. Costero, S. Gil, R. Martínez-Máñez and F. Sancenón, *Org. Biomol. Chem.*, 2014, **12**, 8745–8751.
39 E. Bodio and C. Goze, *Dyes Pigm.*, 2019, **160**, 700–710.
40 D. Lancet and I. Pecht, *Biochemistry*, 1977, **16**, 5150–5157.
41 H. A. A. El-Ali, J. Jing and X. Zhang, *RSC Adv.*, 2019, **9**, 16246–16251.
42 B. Zhu, R. Sheng, T. Chen, J. Rodrigues, Q.-H. Song, X. Hu and L. Zeng, *Coord. Chem. Rev.*, 2022, **463**, 214527.
43 S. Zhang, Y. Wang, F. Meng, C. Dai, Y. Cheng and C. Zhu, *Chem. Commun.*, 2015, **51**, 9014–9017.
44 Y. Sasaki, J. Gautier, M. Li, L. Karmazin, T. W. Ebbesen and C. Genet, *J. Phys. Chem. C*, 2023, **127**, 18526–18532.
45 T. Lee and J. F. Peng, *Cryst. Growth Des.*, 2010, **10**, 3547–3554.
46 H. Sunahara, Y. Urano, H. Kojima and T. Nagano, *J. Am. Chem. Soc.*, 2007, **129**, 5597–5604.
47 W. Chi, J. Chen, W. Liu, C. Wang, Q. Qi, Q. Qiao, T. M. Tan, K. Xiong, X. Liu, K. Kang, Y.-T. Chang, Z. Xu and X. Liu, *J. Am. Chem. Soc.*, 2020, **142**, 6777–6785.
48 D. Li, L. Zong, D. Li, S. Sui, Y. Xiao, B. Zhuang, Y. Shen, Z. Huang and W. Wu, *J. Mater. Chem. C*, 2023, **11**, 4025–4032.
49 S. Zhang, B. Yang, B. Yuan, C. Zhou, M. Zhang, Y. Zhao, P. Ye, L. Li and H. Li, *ACS Sens.*, 2023, **8**, 1220–1229.
50 N. Vijay, S. P. Wu and S. Velmathi, *ACS Appl. Bio Mater.*, 2021, **4**, 7007–7015.
51 Q. Liu, M. Liu, D. Li, K. Li, H. Xu, J. Lu, X. Shao and T. Liu, *Sens. Diagn.*, 2022, **1**, 130–133.
52 K. Liu, J. Zhang, Q. Shi, L. Ding, T. Liu and Y. Fang, *J. Am. Chem. Soc.*, 2023, **145**, 7408–7415.
53 K. Liu, G. Wang, N. Ding, J. Zhang, J. Kong, T. Liu and Y. Fang, *ACS Appl. Mater. Interfaces*, 2021, **13**, 19342–19350.
54 R. Huang, T. Liu, H. Peng, J. Liu, X. Liu, L. Ding and Y. Fang, *Chem. Soc. Rev.*, 2024, **53**, 6960–6991.
55 Z. Wang, K. Liu, X. Chang, Y. Qi, C. Shang, T. Liu, J. Liu, L. Ding and Y. Fang, *ACS Appl. Mater. Interfaces*, 2018, **10**, 35647–35655.
56 K. Liu, C. Shang, Z. Wang, Y. Qi, R. Miao, K. Liu, T. Liu and Y. Fang, *Nat. Commun.*, 2018, **9**, 1695.
57 J. Zhao, M. Qin, J. You, K. Liu, L. Ding, T. Liu, J. Kong and Y. Fang, *Dyes Pigm.*, 2022, **197**, 109870.